JGR Oceans

RESEARCH ARTICLE
10.1029/2024JC021342

Ice Shelf Water-Influenced Fast Ice and Sub-Ice Platelet Layer Near the Campbell Ice Tongue, Terra Nova Bay

G. M. Brett[1], N. B. Gardiner[1,2], P. J. Langhorne[3], W. Rack[1], C. Haas[4,5,6,7], A. Irvin[5,8], and S. Kim[9]

[1]Gateway Antarctica, University of Canterbury, Christchurch, New Zealand, [2]Antarctica New Zealand, Christchurch, New Zealand, [3]Department of Physics, University of Otago, Dunedin, New Zealand, [4]Department of Earth and Atmospheric Science, University of Alberta, Edmonton, AB, Canada, [5]Department of Earth and Space Science and Engineering, York University, Toronto, ON, Canada, [6]Alfred Wegener Institute for Polar and Marine Research, Bremerhaven, Germany, [7]Department of Environmental Physics, University of Bremen, Bremen, Germany, [8]Department of Geography, Memorial University of Newfoundland, St. John's, NL, Canada, [9]Division of Life Sciences, Korean Polar Research Institute (KOPRI), Incheon, Republic of Korea

Key Points:

- Basal melt of the Campbell Ice Tongue is a significant source of Ice Shelf Water in north Terra Nova Bay
- Thickness distributions of fast ice and the sub-ice platelet layer were used to infer Ice Shelf Water outflow from the Campbell Ice Tongue
- Fast ice in north Terra Nova Bay is stabilized by the Campbell Ice Tongue and broken up by the Terra Nova Bay Polynya

Correspondence to:
G. M. Brett,
gemma.brett@canterbury.ac.nz

Citation:
Brett, G. M., Gardiner, N. B., Langhorne, P. J., Rack, W., Haas, C., Irvin, A., & Kim, S. (2025). Ice shelf water-influenced fast ice and sub-ice platelet layer near the Campbell Ice Tongue, Terra Nova Bay. *Journal of Geophysical Research: Oceans*, *130*, e2024JC021342. https://doi.org/10.1029/2024JC021342

Received 14 MAY 2024
Accepted 13 OCT 2025

Author Contributions:
Conceptualization: G. M. Brett, N. B. Gardiner, P. J. Langhorne, W. Rack, C. Haas, A. Irvin
Data curation: G. M. Brett
Formal analysis: G. M. Brett
Funding acquisition: G. M. Brett, P. J. Langhorne, W. Rack, C. Haas, A. Irvin, S. Kim
Investigation: G. M. Brett, N. B. Gardiner
Methodology: G. M. Brett, W. Rack, C. Haas, A. Irvin
Project administration: G. M. Brett, N. B. Gardiner, S. Kim
Resources: G. M. Brett, P. J. Langhorne, W. Rack, C. Haas, S. Kim
Software: A. Irvin
Supervision: G. M. Brett, S. Kim
Validation: G. M. Brett, N. B. Gardiner
Visualization: G. M. Brett
Writing – original draft: G. M. Brett, P. J. Langhorne

Abstract Here, we present the first dedicated in situ measurements of the thickness distributions of fast ice and the sub-ice platelet layer, formed by supercooled Ice Shelf Water in north Terra Nova Bay, Antarctica. With the objective of inferring source regions and circulation of Ice Shelf Water, we measured fast ice and sub-ice platelet layer thickness distributions near the Campbell Ice Tongue in late spring of 2021, using drill hole surveys and high-resolution ground-based electromagnetic induction soundings. We observed thicker fast ice and sub-ice platelet layer near the ice tongue with very thick and narrow sub-ice platelet layer maxima indicating highly channeled outflow of supercooled Ice Shelf Water from beneath the ice tongue directed by ice mélange, subglacial formations, and grounded regions. We conclude that a significant volume of supercooled Ice Shelf Water is locally sourced from the Campbell Ice Tongue through basal melting and affirm that the icescape in north Terra Nova Bay results from a complex interplay of glacial morphology, polynya forcing, and ocean circulation.

Plain Language Summary Fresh meltwater from glacial ice on the Antarctic continent can influence coastal sea ice formation. If the meltwater forms deep in the ocean, it can be supercooled and freeze into platelet ice crystals, which contribute to sea ice formation and form thick layers beneath sea ice called sub-ice platelet layers (SIPL). Platelet ice, a crystallographic signature of supercooled glacial meltwater provides important information on difficult to observe interacting processes occurring between the atmosphere, glacial ice, the ocean, and sea ice along the Antarctic coast. In late spring of 2021, we carried out detailed surveys of glacially influenced coastal sea ice and SIPL beside the Campbell Ice Tongue in north Terra Nova Bay, Ross Sea, Antarctica, with high-resolution geophysical surveying. Our objective was to use sea ice and SIPL distributions to infer where the glacial meltwater was coming from and where it circulates. Our surveys revealed thicker sea ice and SIPL near the ice tongue with thick bands of SIPL indicating highly channeled outflow of supercooled glacial meltwater from beneath the Campbell Ice Tongue through glacial formations. We conclude that a significant volume of supercooled glacial meltwater in north Terra Nova Bay is locally sourced from the Campbell Ice Tongue through basal melting.

1. Introduction

On the Antarctic coastline, land-fast sea ice (henceforth referred to as fast ice) is an important interface between land ice and the open ocean (Giles et al., 2008; Massom et al., 2018) that affects ice sheet mass balance by stabilizing and buttressing ice tongues (Gomez-Fell et al., 2022, 2024; Massom et al., 2010) and ice shelves (Greene et al., 2018) from ocean swell (Christie et al., 2022; Massom et al., 2018). Land ice, in turn, provides a margin for fast ice to attach to and affects fast ice formation through melt processes and freshwater input to the ocean (Fraser et al., 2023). Fast ice, ice shelves, and ice tongues are key features for the formation of coastal polynyas (Fraser et al., 2019; Nihashi & Ohshima, 2015).

A potentially supercooled water mass called Ice Shelf Water (ISW) is formed from basal melting at the grounding zones of ice shelves and outlet glaciers (Jacobs et al., 1985) by High Salinity Shelf Water (HSSW) produced in coastal polynyas (Nakata et al., 2015). As buoyant ISW rises from deep under ice shelves and outlet glaciers, it

Writing – review & editing: G. M. Brett, N. B. Gardiner, P. J. Langhorne, W. Rack, C. Haas, A. Irvin

becomes in situ supercooled (Foldvik & Kvinge, 1974; Jenkins & Bombosch, 1995) and precipitates frazil ice (Holland & Feltham, 2005). ISW promotes sea ice growth by stabilizing the upper water column (Hellmer, 2004), or if in situ supercooled, through heat loss to the ocean (Gough et al., 2012). Frazil ice grows into larger platelet ice crystals (Smith et al., 2012), which can be deposited beneath sea ice and incorporated with congelation growth, augmenting sea ice thickness (Purdie et al., 2006). Once the deposition of platelet ice outpaces congelation growth, an unconsolidated mass of crystals called a sub-ice platelet layer (SIPL) can form beneath sea ice (Gough et al., 2012; Wongpan et al., 2015, 2021).

Studies of ISW-influenced fast ice and SIPL have linked late-spring volumes of platelet ice, within fast ice and SIPL, to supercooled ISW outflow in Atka Bay, Weddell Sea (Hoppmann, Nicolaus, Hunkeler, et al., 2015; Hoppmann, Nicolaus, Paul, et al., 2015), and McMurdo Sound (Langhorne et al., 2015). The thickness distribution of SIPL reflects the circulation and degree of in situ supercooling of the ocean beneath (Hughes et al., 2014; Wongpan et al., 2021). Multiple years of ground-based (Brett et al., 2020) and airborne (Haas et al., 2021) electromagnetic induction (EM) assessments of ISW-influenced fast ice and SIPL thickness distributions in McMurdo Sound were correlated with supercooled ISW circulation (Hughes et al., 2014; Lewis & Perkin, 1985; Robinson et al., 2014) from the McMurdo-Ross Ice Shelf Cavity. This relationship allowed interannual and diurnal variability of SIPL thickness to be linked to polynya activity in the western Ross Sea (Brett et al., 2020) and the oscillation of the tides (Brett et al., 2024). An extensive airborne electromagnetic induction (AEM) survey of fast ice along the Victoria Land Coastline identified that marine-terminating outlet glaciers and ice tongues also contribute to the formation of in situ supercooled ISW and platelet ice in the western Ross Sea (Langhorne et al., 2023).

Crystallographic signatures of in situ supercooled ISW in the form of marine, frazil, and platelet ice have been observed in Terra Nova Bay, western Ross Sea, beneath ice shelves, ice tongues, and fast ice (refer to Figure 1a for locations). ISW is abundant in the region (Budillon & Spezie, 2000; Yoon et al., 2020) but so far its sources have not been definitively constrained. In north Terra Nova Bay, marine ice (Souchez et al., 1995) and basal freezing (Han & Lee, 2015) occur beneath the Campbell Ice Tongue (Figure 1). Beneath adjoining fast ice, a SIPL was detected in biological studies in late spring of 2002, 2005, and 2006 (Vacchi et al., 2004, 2012) and in AEM surveys in late spring of 2017 (Langhorne et al., 2023). The presence of marine ice and SIPL signals that in situ supercooled ISW is circulating in the region, which the AEM surveys indicated could be locally sourced from the ice tongue (Langhorne et al., 2023). However, no dedicated in situ investigation of the influence of ISW on fast ice, the SIPL, and the Campbell Ice Tongue in north Terra Nova Bay has been carried out. This information is important given that the ice tongue is thinning (Han & Lee, 2015) and decreasing in area (Han et al., 2022) with major effects expected for adjoining fast ice and local ecosystems.

Here, we assess spatial distributions of ISW-influenced fast ice and SIPL near the Campbell Ice Tongue to infer the pattern of supercooled ISW circulation in north Terra Nova Bay and the effects of local geomorphological features including subglacial morphology and grounded regions of the ice tongue. To investigate the processes influencing fast ice in north Terra Nova Bay, we used satellite imagery to observe fast ice, ice tongue, and polynya interactions during the winter of 2021. In the following late spring of 2021, we assessed thickness distributions of ISW-influenced fast ice and SIPL with drill hole and single-frequency electromagnetic induction (EM) sounding surveys. As observed in McMurdo Sound, the spatial distributions of thicker ISW-influenced fast ice and SIPL in Terra Nova Bay should reflect supercooled ISW circulation. We describe the study area in Section 2, methods in Section 3, and results in Section 4. In Section 5, we discuss our findings in a regional context considering prior oceanographic observations in Terra Nova Bay.

2. Study Area

2.1. Terra Nova Bay

Terra Nova Bay is bound by the Drygalski Ice Tongue in the south, the Nansen Ice Shelf in the west, and a large embayment in the north (Figure 1a). The Terra Nova Bay Polynya (Figure 1a) occurs in the region, producing 10% of sea ice (Kurtz & Bromwich, 1985), and 33% of HSSW (Fusco et al., 2009; Rusciano et al., 2013) in the Ross Sea (Rusciano et al., 2013). HSSW formed within the polynya (Thompson et al., 2020) is thought to drive basal melting at depth in the grounding zones of the Nansen Ice Shelf and larger outlet glaciers in the region forming ISW (Budillon & Spezie, 2000; Yoon et al., 2020). Cyclonic circulation transports ISW to the northeast (Figure 1a) (Cappelletti et al., 2010; Yoon et al., 2020) with ISW observed extensively in Terra Nova Bay at

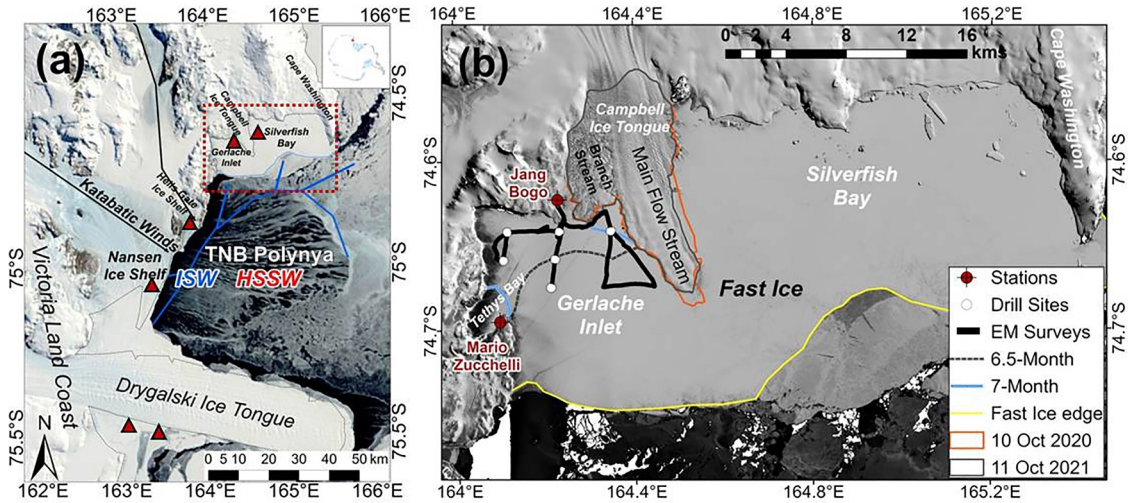

Figure 1. (a) Prior observations of SIPL and marine ice (red triangles) near ice shelves and ice tongues in Terra Nova Bay, located on the Victoria Land Coastline in the northwestern Ross Sea (see inset (Gerrish et al., 2022)). The Terra Nova Bay (TNB) Polynya, evident in this MODIS image from 4 November 2021, is shown with cyclonic circulation of ISW (blue lines) conjectured from Budillon and Spezie (2000). The red box shows the location of (b) the study area with outlines of the Campbell Ice Tongue area on 10 October 2020 (orange) and 11 October 2021 (dark gray). Fast ice sections are shown with drill sites (white circles), EM survey tracks (black line), and the Italian "Mario Zucchelli" and Korean "Jang Bogo" research stations (red crossed circles) on a Landsat-8 panchromatic image (5 November 2021).

depths of 30–600 m, being deepest and most abundant near the Nansen Ice Shelf (Budillon & Spezie, 2000; Yoon et al., 2020). In the northeast, a narrow tongue of ISW at shallower depths, located southeast of Gerlache Inlet, was consistently observed in multiple years of oceanographic profiling (Budillon & Spezie, 2000).

2.2. Campbell Ice Tongue Embayment

The Campbell Glacier flows from the Transantarctic Mountains into an embayment in north Terra Nova Bay where it forms the Campbell Ice Tongue (Figure 1). The ice tongue consists of a fast flowing "main flow" stream (~14 km long, ~5 km wide) and a smaller "branch stream" to the west (8 km long, 2.5 km wide) (Figure 1b) made up of ice mélange (Han & Lee, 2014). It has a ~14-km long U-shaped grounding line (Figure 1b) (Han & Lee, 2014). The main flow stream is grounded in the southwest near the ice tongue terminus (Figure 2) (Han & Lee, 2014) and forms an ice rumple (Han et al., 2022). The branch stream is grounded in the east and west (Figure 2) (Han & Lee, 2014) on bedrock (Souchez et al., 1995). Radio Echo Sounding of the ice tongue in 1999 showed a rippled undersurface and thicknesses of 200–300 m for most of its length, increasing to 700 m in the grounding zone (Bianchi et al., 2001).

The southward protruding ice tongue splits north Terra Nova Bay into Gerlache Inlet in the west and Silverfish Bay in the east (Figure 1b). Gerlache Inlet is 10–12 km from east to west and 13 km from north to south and includes Tethys Bay. Silverfish Bay is 25 km from east to west and 12 km from north to south. Multibeam bathymetry (Figure 2a) collected in Gerlache Inlet (Jung et al., 2021; Lee et al., 2022) revealed complex seafloor morphology with deep troughs, ridges, and a seabed rise near the ice tongue. Numerous smaller deep (~500 m) channels run from beneath the main flow stream of the ice tongue.

We were unable to source any detailed oceanographic assessments in the study region. In the winter of 2000, near supercooled ocean temperatures were observed to the south of Tethys Bay (Cappelletti et al., 2010). Tides in the region are diurnal with a maximum range of 0.60 m (Han & Lee, 2014) with strong tidal currents expected for the coastal morphology and bathymetry in Gerlache Inlet (Han & Lee, 2018). The Terra Nova Bay Polynya can occur within the study region when open water dominates in early winter. Once fast ice is established, the polynya occurs along the fast ice edge and should influence ocean circulation in the region.

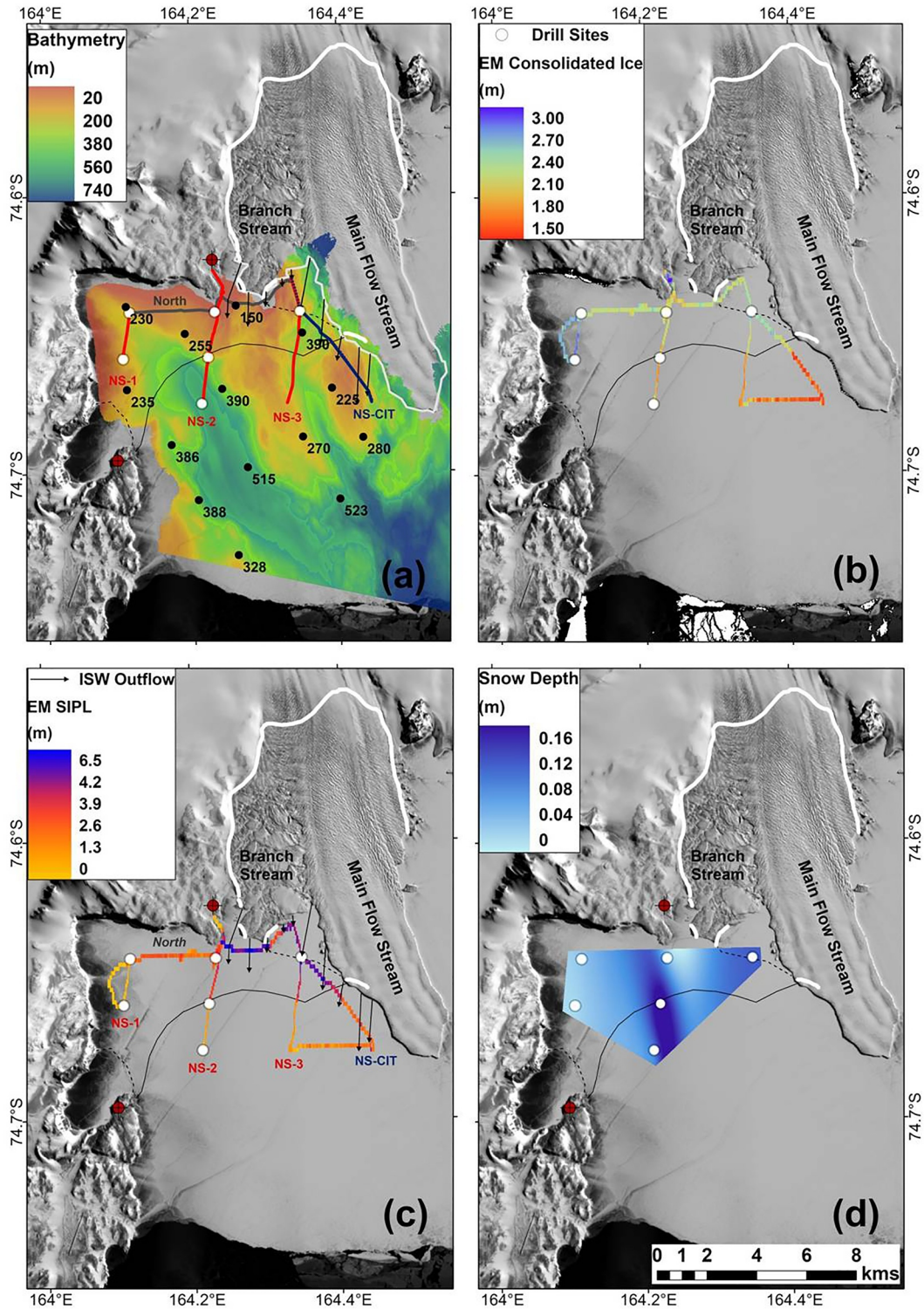

Figure 2. (a) Multibeam bathymetry and depth measurements (Jung et al., 2021; Lee et al., 2022) with the *North* and *NS*- EM transects shown in Figures 4–6, (b) EM consolidated ice thickness, (c) EM SIPL thickness, and (d) snow depth interpolated from drill sites displayed on a Landsat-8 panchromatic image (5 November 2021). Grounded regions of the ice tongue (Han et al., 2022) are shown as white lines and conjectured ISW outflow from the ice tongue illustrated as black arrows in (a) and (c). Black solid (dashed) line denotes the edge of fast ice in place for 6.5 (7) months.

2.3. Fast Ice and Sub-Ice Platelet Layer in North Terra Nova Bay

Fast ice consistently forms in Gerlache Inlet and Silverfish Bay with a SIPL first observed in biological studies (Vacchi et al., 2004, 2012). In late spring of 2005 and 2006, extensive surveys of Antarctic silverfish egg distribution with respect to the occurrence of platelet ice were carried out (Vacchi et al., 2012), which revealed high abundance near the ice tongue in both bays where the fast ice was thick (~2.5 m). In November 2017, AEM surveys detected thicker fast ice and SIPL near the ice tongue and northern coastline in both bays with more abundant SIPL observed east of the ice tongue in Silverfish Bay (Langhorne et al., 2023). Maximum AEM-measured SIPL thicknesses near the coast were 2.1 and 1.6 m, east and west of the ice tongue, respectively. Point observations in the region recorded fast ice thicknesses of 2.4–2.5 m near the coast in Gerlache Inlet (Guglielmo et al., 2007; Vacchi et al., 2004). Near Tethys Bay, fast ice and SIPL thickness were, respectively, 1.4 m and 0.8–1.2 m in spring of 1997 (Guglielmo et al., 2007) and 2.4 m and 0–2 m in spring of 1999 (Lazzara et al., 2007).

3. Methods

To characterize the late-spring fast ice conditions, we monitored fast ice formation in Gerlache Inlet and Silverfish Bay during winter and spring (March–November) of 2021 with synthetic aperture radar (SAR) (Sentinel-1) and optical (Landsat-8 and Moderate Resolution Imaging Spectroradiometer (MODIS)) images, when available. In late spring of 2021 (3–7 November), the thickness distributions of snow, fast ice, and the SIPL were then surveyed with drill hole and single-frequency electromagnetic induction (EM) measurements (Brett et al., 2025a, 2025b) over ~60 km^2 of fast ice in Gerlache Inlet as shown in Figure 1b.

At drill sites, two 30 m cross-profiles were laid out in north-south and east-west directions. Sea ice and SIPL thicknesses were measured in five drill holes, made at the center and end points of each line, using a tape measure with weighted bar, and applying the resistance method (Price et al., 2014). Mean values and standard deviations were calculated for each drill site. At the drill site furthest to the southwest, only three drill hole measurements were made due to weather conditions. Snow depth was measured at 0.5 m intervals along each cross-profile using a ruler (cm accuracy). The ~120 snow depth measurements were averaged to provide a mean value at each drill site and then spline interpolated using first-derivative minimum-curvature (no smoothing) to approximate snow distribution in the region (Figure 2d).

EM surveys of fast ice and SIPL thickness distributions were carried out using a single-frequency (9.8 kHz and 3.66 m coil-spacing) Geonics Ltd. EM31-MK2 instrument mounted on a sledge and towed by a vehicle. We configured the EM31 to sample at 1 Hz resulting in a geo-located measurement every ~5 m at typical travel speeds. EM measurements were made for 20 s over each of the 28 drill holes. A total distance of 39 km was surveyed with EM. We used the processing method from Irvin (2018) applied in McMurdo Sound (Brett et al., 2020, 2024) to obtain sea ice and SIPL thicknesses from the in-phase and quadrature components of single-frequency EM.

An electromagnetic forward model was run to compute the EM response over a layered subsurface. The model included three horizontal conductive layers with a range of thicknesses and conductivities: (1) consolidated ice thickness (i.e., sea ice plus the snow layer) (0.5–6 m; 0 mS m^{-1}), (2) SIPL (0–15 m; 100–1,500 mS m^{-1}), and (3) seawater (2,400–3,000 mS m^{-1}). A "brute force" inversion was applied, which compared EM in-phase and quadrature readings at drill holes with theoretical forward modeled values to obtain the best-matching bulk SIPL conductivity model, as determined by root mean square error (RMSE) between drill hole and inverted thicknesses. EM inverted sea ice (Figure 2b) and SIPL thicknesses (Figure 2c) were then linearly interpolated.

Given that seawater conductivity in the region was unconstrained, we ran multiple inversions with fixed seawater conductivities and looped through a range of SIPL conductivities from 100 to 1,500 mS m^{-1} in 50 mS m^{-1} increments. We did this individually for each seawater conductivity from 2,400 to 3,000 mS m^{-1} in 100 mS m^{-1} increments. An optimum SIPL bulk conductivity of 600 mS m^{-1} was consistently returned. We then ran inversions with a fixed SIPL bulk conductivity of 600 mS m^{-1} for the same range of seawater conductivities, resulting in an optimum value of 2,700 mS m^{-1} determined from the RMSE for the entire study region (Figure 3a).

In this study, snow measurements covered a smaller area than EM surveys, and we could not account for the contribution of the snow layer to EM consolidated ice thickness. However, snow measured at drill sites and

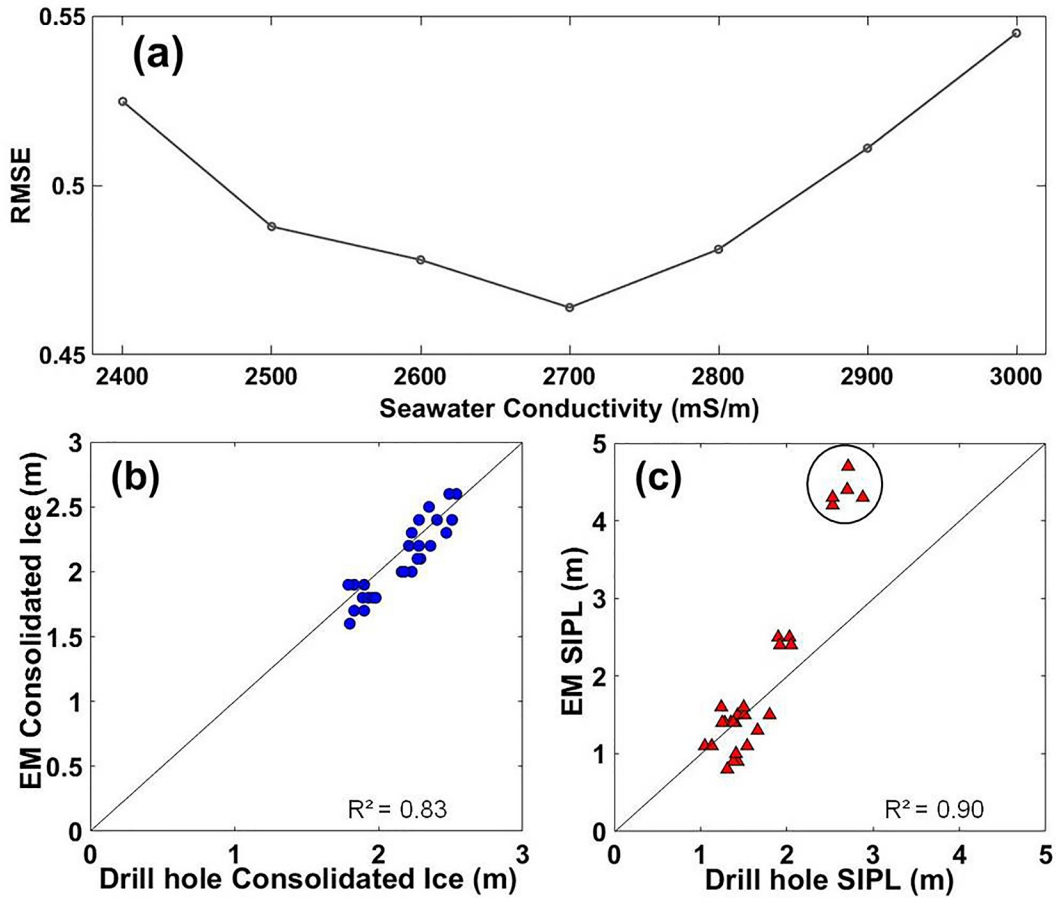

Figure 3. (a) RMSE values from EM inversions showing an optimal seawater conductivity of 2,700 mS m^{-1} for a fixed SIPL bulk conductivity of 600 mS m^{-1} and a range of seawater conductivities (2,400–3,000 mS m^{-1}). Comparison of coincident inverted EM (at drill holes) and drill hole measurements of (b) consolidated ice (sea ice plus snow) and (c) SIPL thickness with R^2 values from linear fits.

sighted along EM tracks was generally thin and loosely packed. The mean snow depth of the 28 drill holes was 0.08 ± 0.05, 3.7% of the mean drill hole-measured consolidated ice thickness (2.17 ± 0.25 m). We thus expect the addition of snow to be ≤0.10 m or <5% of EM consolidated ice thickness and negligible.

The combined thicknesses of consolidated ice and SIPL affect the error of the inversion to a mean relative value of ∼10%, for thicknesses of either layer over 2 m (Irvin, 2018). When consolidated ice and SIPL are very thin or thick, they occupy a sensitive region of the forward model where a small change in the EM response can produce large changes in inverted thicknesses. This limitation and its implications for the inversion of consolidated ice when a thin SIPL is present are described in further detail in Section 3.1 and Figure 2c of Brett et al. (2024).

Figures 3b and 3c show a 1:1 comparison of drill hole-measured consolidated ice and SIPL thicknesses with spatially coincident EM thicknesses inverted from the model. R^2 values for linear fits of EM versus drill hole thicknesses were 0.83 for consolidated ice and 0.90 for SIPL, the latter having a wider range. The mean drill hole (EM) measured thicknesses at drill holes were 2.17 ± 0.25 m (2.09 ± 0.27 m) for consolidated ice and 1.77 ± 0.53 m (2.04 ± 1.22 m) for SIPL. Most of the drill hole data plotted near the 1:1 lines (Figures 3b and 3c) with deviations that demonstrated that the inverted seawater (2,700 mS m^{-1}) and SIPL (600 mS m^{-1}) conductivities were representative of conditions in the study region. A mean deviation of −3.7% for consolidated ice and +10.7% for SIPL was observed with EM relative to drill hole thickness.

However, five EM SIPL thicknesses (circled in Figure 3c) measured at a drill site nearest the ice tongue in the northeast (Figure 1b) were 1.4–2 m greater than the coincident drill hole measurements. In contrast, consolidated ice thicknesses at this site matched closely with a small mean deviation of +0.04 m for EM versus drill hole

measurements. The relatively large difference between EM and drill hole-measured SIPL thicknesses suggested a shift in the subsurface conductivity near the ice tongue, potentially caused by a change in seawater conductivity.

We queried this by running multiple forward models, with seawater conductivities ranging from 1,000 to 2,400 mS m^{-1} and SIPL conductivities from 100 to 1,000 mS m^{-1}, for the five drill holes made at this site. The optimum SIPL bulk conductivity was consistently 600 mS m^{-1} for this seawater range. We then ran multiple forward models for a fixed SIPL bulk conductivity of 600 mS m^{-1} and a seawater conductivity range of 1,000–2,400 mS m^{-1}. An optimum seawater conductivity of 1,300 mS m^{-1} was inverted, which corresponded to a salinity of 15.5 (for a temperature −1.9°C and pressure of 15 dbar) (McDougall & Barker, 2011).

We thus interpreted absolute magnitudes of EM SIPL thickness in the northeast region near the ice tongue with caution because they could be overestimated. However, the main objective of this study was to constrain and quantify the late-spring distributions of ISW-influenced fast ice and SIPL thickness and we were confident from previous experience that the EM method did this well.

4. Results

4.1. Fast Ice Formation

Satellite observations revealed that the fast ice from the previous year broke out from Gerlache Inlet and Silverfish Bay. This was immediately followed by the calving of the ice tongue from the terminus and eastern flank as shown in Figure 1b by the difference in the ice tongue area in October 2020 and 2021. In early March 2021, sea ice began to form in the study region and polynya activity increased. During calm periods, thermodynamic sea ice growth was observed with fast ice forming attached to the coastline, ice tongue, and Cape Washington. Newly formed fast ice was frequently broken up and circulated eastward by the polynya where it coalesced along the western margins of the ice tongue and Cape Washington.

In early November 2021, the fast ice in north Terra Nova Bay was extensive and entirely first-year in composition. In Gerlache Inlet, the fast ice was made up of three sections (ages) as shown in Figure 1b: Tethys Bay and northeast section (7-month), coastal fringe (6.5-month), and southern section (4.5-month). Fast ice in Gerlache Inlet first persisted from 28 March 2021 in Tethys Bay and in the northeast between the branch and main flow streams (i.e., north of the 7-month line). In mid-April, fast ice reached as far south as the ice tongue terminus in both bays. In mid-June, polynya forcing caused an extensive breakout of 2-month old fast ice in Gerlache Inlet. The remaining fast ice consisted of a 3–6 km wide fringe attached to the coastline and ice tongue (i.e., north of the 6.5-month line in Figure 1b) over shallower bathymetry (0–300 m) (Figure 2a). Fast ice to the south of this coastal fringe persisted from late-June and had been established for 4.5-month when surveyed in early November.

4.2. Thickness Distributions of Fast Ice and Sub-Ice Platelet Layer

Figure 2 shows the thickness distributions of EM measured consolidated ice and SIPL and snow depth (measured at drill sites) in early November 2021. The EM surveys (∼5 m sample spacing) detected the thickest consolidated ice (Figure 2b) and SIPL (Figure 2c) in the northeast near the ice tongue, with thicknesses decreasing to the south and west. EM consolidated ice (Figure 2b) was also thick in the far west where the ice was bare of snow. We observed the thinnest consolidated ice on the 4.5-month fast ice in the southeast and the thinnest SIPL in west Gerlache Inlet. Mean EM consolidated ice and SIPL thicknesses from all EM surveys were, respectively, 2.14 ± 0.31 m and 2.17 ± 1.52 m. Differences in thickness with respect to ice age were apparent, with thinner mean EM consolidated ice (1.82 m) and EM SIPL (1.39 m) measured on the younger 4.5-month fast ice versus the older 6.5-month section, with respective mean thicknesses of 2.35 and 2.72 m.

The lower resolution drill hole point measurements captured the same pattern in fast ice and SIPL thickness distributions. Mean drill hole-measured fast ice thickness was 2.09 ± 0.27 m for the entire survey region, ranging from 2.40 m at the drill site in the northeast near the ice tongue (i.e., 6.5-month old fast ice), 2.25 m in the west where the ice was bare of snow, to 1.76 m in the center and south. Mean drill hole-measured SIPL thickness was 1.70 ± 0.54 m, varying from 2.67 m in the northwest to 1.30 m in the west.

Snow coverage in Gerlache Inlet (Figure 2d) was thin, wind-distributed, and had a flat surface. Mean snow depth at drill sites was 0.08 ± 0.05 m and ranged from bare ice in the west, deeper snow in the center (0.16 m), and thinner coverage (0.09 m) in the east and northeast.

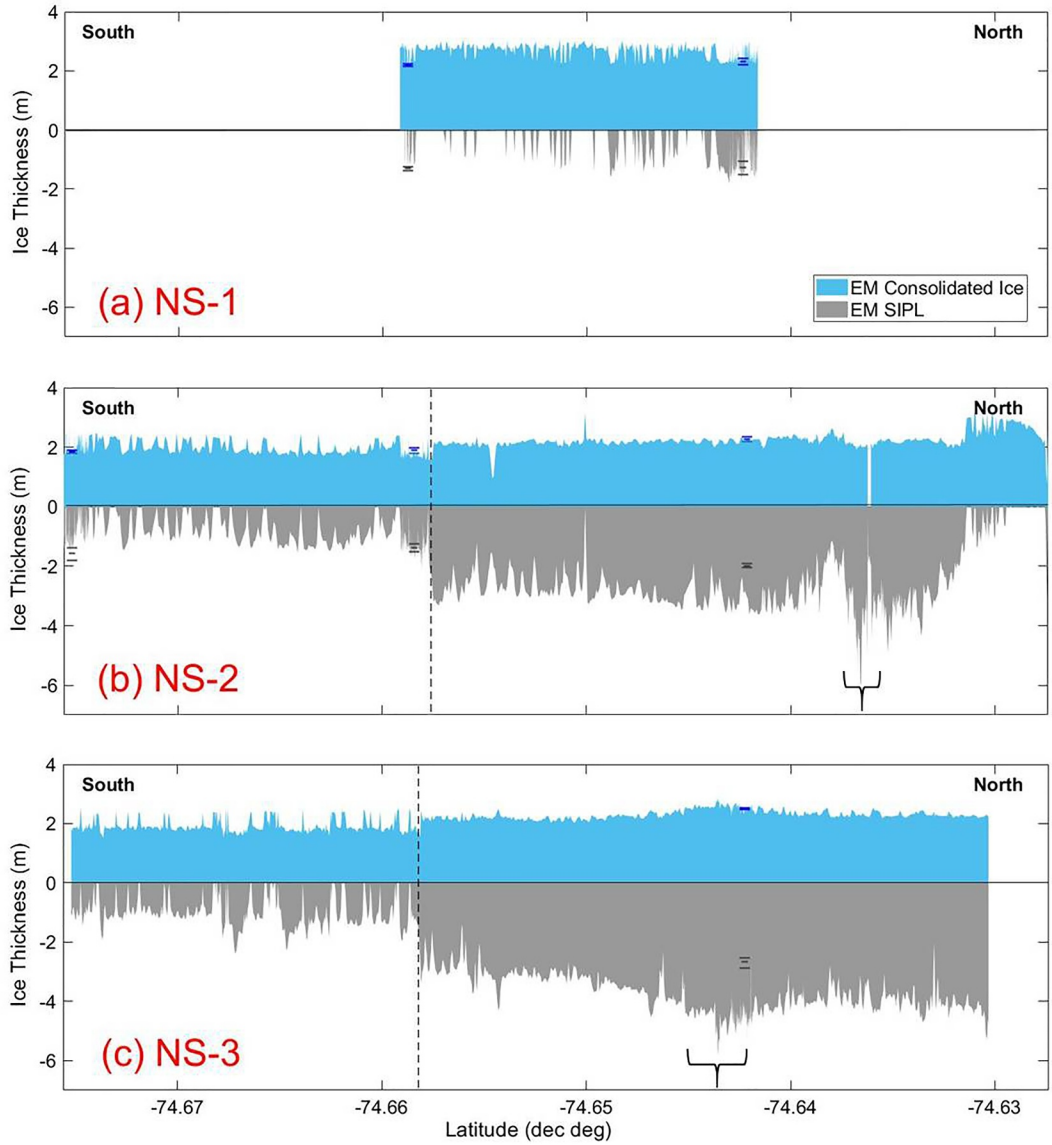

Figure 4. Parallel north-south EM transects (spaced from west to east at 3.5 km distance) of consolidated ice (positive *y*-axis) and SIPL thickness (negative *y*-axis) with maxima mentioned in the text demarcated with corresponding maximum, minimum, and mean drill hole measurements (illustrated by horizontal dashes), on (a) *NS-1*, (b) *NS-2*, and (c) *NS-3*. The vertical stippled lines show the transition between the 4.5 (south) and 6.5-month (north) old fast ice sections.

The EM transects in Figures 4 and 5 show that SIPL thickness increased from west to east across Gerlache Inlet, toward the ice tongue, on both the 6.5 and 4.5-month sections. Toward the ice tongue in the north, consolidated ice and SIPL thicknesses displayed the same increasing trend on the *NS-2*, *NS-3* (Figure 4), and *NS-CIT* (Figure 5) transects. On the same transects, sharp decreases in consolidated ice and SIPL thickness were observed on the transition from the 6.5 to 4.5-month fast ice. The *North* transect (Figure 6) revealed substantial thicknesses of both consolidated ice and SIPL adjacent to the ice tongue in the east.

For reasons discussed in Sections 3 and 5.1, we interpreted absolute magnitudes of EM SIPL thicknesses in the northeast near the ice tongue with caution. Additionally, on all EM transects, the effect of the inversion over thin SIPL (<0.5 m) (as described in Section 3) was evident and manifested as sharp spikes in consolidated ice thickness and covariance with SIPL thickness. From previous experience of this effect in McMurdo Sound (refer to Brett et al., 2024), we interpreted the spikes in EM consolidated ice thickness as an unwanted effect and EM SIPL thickness variability as a real observed effect. True EM consolidated ice thicknesses thus generally

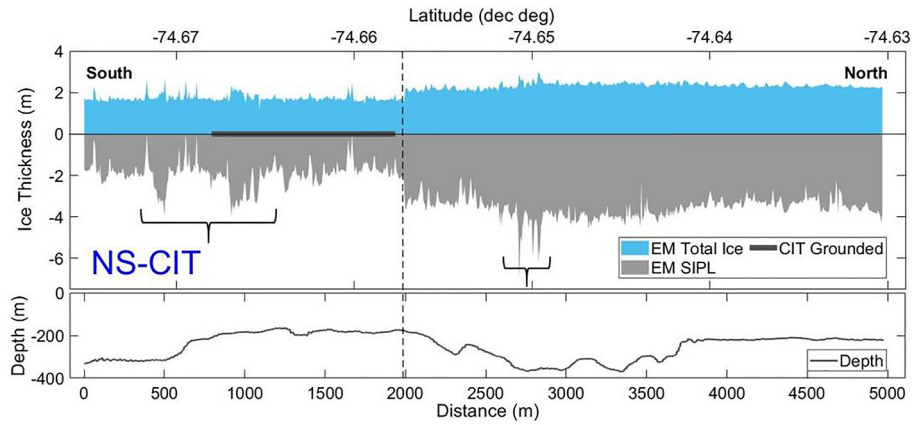

Figure 5. The north-south *NS-CIT* EM transect (upper panel) of consolidated ice (positive *y*-axis) and SIPL thickness (negative *y*-axis) with maxima mentioned in the text demarcated and bathymetric depth (lower panel) extracted from Jung et al. (2021). Dashed vertical lines show the transition between the 4.5 and 6.5-month old fast ice sections with the estimated extent of the adjacent grounded region of the main flow stream to the east from Han et al. (2022).

corresponded to smaller magnitude EM thickness measurements as shown by comparison with the range of coincident drill hole-measured thickness at sites (Figures 4 and 6).

The *NS-1* transect in Figure 4a revealed thick fast ice (2.3 m) and thin SIPL (0–1.9 m) in the west. The thickest SIPL on this transect was observed near the northern coastline with isolated pockets of SIPL (1.4–1.9 m) along the profile.

The *NS-2* transect (Figure 4b) showed thick consolidated ice of ∼2–2.2 m and consistently thick SIPL (2–4 m) under the 6.5-month fast ice section. A 5–6 m SIPL maxima centered at latitude −74.636° (Figure 4b) was observed east of the branch stream (Figure 2c). On the 4.5-month fast ice, consolidated ice was ∼1.7 m and SIPL thicknesses varied from 0 to 1.5 m.

On the *NS-3* transect (Figure 4c), a thick SIPL maxima (centered at −74.643°) with thicker overlying consolidated ice (2.6–2.8 m) was observed. In the far north (toward latitude −74.63°), SIPL increased in thickness between the branch and main flow streams (Figure 2c). On the younger ice, consolidated ice and SIPL thicknesses were thinner with several SIPL maxima of 2.2–2.4 m thickness and 100–130 m width observed.

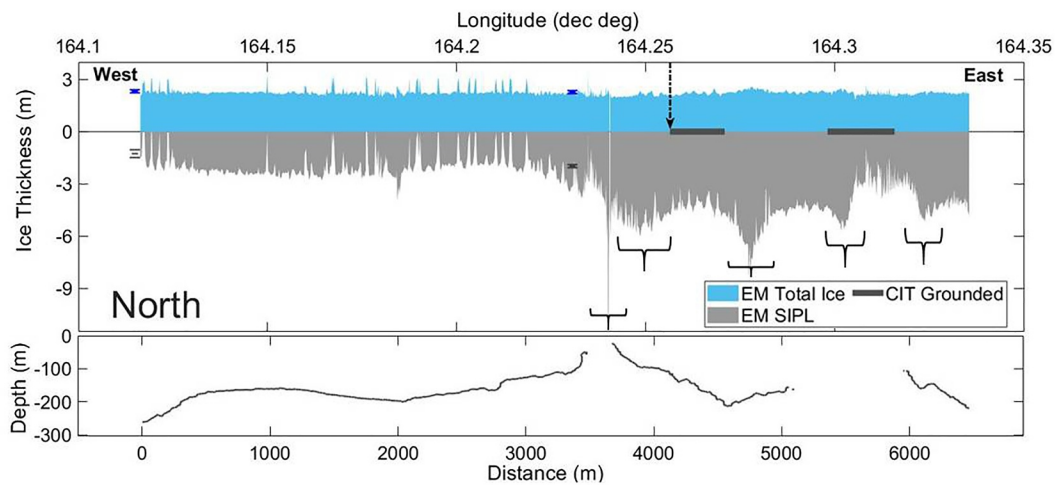

Figure 6. The *North* alongshore EM transect (upper panel) of consolidated ice (positive *y*-axis) and SIPL thickness (negative *y*-axis) with maxima mentioned in the text demarcated and bathymetric depth (lower panel) extracted from Jung et al. (2021). The dashed vertical arrow shows the western extent of the branch stream and horizontal gray lines, the estimated locations of grounded regions of the ice tongue to the north from Han et al. (2022).

The *NS-CIT* transect in Figure 5 was carried out ~0.5–1 km from the ice tongue and partially adjacent to the *NS-3* transect in the north (Figure 2a). On the 6.5-month fast ice, consolidated ice thickness was ~2.5 m in the north and up to 3 m over narrow SIPL maxima. Over deeper bathymetry (300–400 m), the SIPL was thicker with 3 maxima of ~50 m width (centered at latitude −74.65°) observed over a short distance (~200 m). The transition to the 4.5-month old fast ice occurred north of where the ice tongue was grounded (location indicated on Figure 5). The younger fast ice had consolidated ice thickness of ~1.7 m and SIPL thickness of ~2 m with prominent SIPL maxima with thicker overlying fast ice (2.3–2.4 m) observed in narrow bands of ~100–150 m width.

The 6.5 km long *North* EM transect in Figure 6 detected SIPL along the entire northern coast with several very thick and narrow accumulations in front of the branch stream of the ice tongue. On the western side of this transect, mean consolidated ice thickness was 2.2 m and SIPL varied from 2 to 3 m. In the center, SIPL was thicker with a very narrow (~15 m wide) and potentially thick SIPL maxima (4–12 m) observed over shallow depths (<25 m) east of the branch stream. In the east, the SIPL was significantly thicker than the west with four SIPL maxima with thicker overlying consolidated ice observed due south of the branch stream. We estimated the widths of the SIPL maxima to be 100–500 m. To the south of the 0.5-km grounded region in the east (location indicated on Figure 6), the SIPL was substantially thinner.

5. Discussion

5.1. EM Inverted Consolidated Ice and SIPL Thicknesses

The mean deviations of coincident EM and drill hole-measured consolidated (−3.7%) and SIPL (+10.7%) thicknesses (Figures 3c and 3b) were within the expected error of the inversion (Irvin, 2018). Given that the mean snow depth at drill sites was <5% of the mean drill hole consolidated ice thickness, we considered EM measured consolidated ice thickness as a good approximation of true fast ice thickness, except where the SIPL was less than 0.5 m in thickness. The close agreement of most EM and drill hole measurements provided confidence that the conductivities of the SIPL (600 mS m^{-1}) and seawater (2,700 mS m^{-1}) were mostly representative of conditions in Gerlache Inlet.

The large deviation of drill hole-measured and EM SIPL thicknesses and low seawater conductivity of 2,700 mS m^{-1} inverted at the drill site in the northeast suggested abundant fresh water in the upper surface ocean in this region near the ice tongue, corroborating high basal melt rates of the ice tongue deduced from SAR interferometry (Han & Lee, 2015). However, the low seawater conductivity was inverted from only five coincident drill hole and EM measurements and would require oceanographic assessment to be conclusive.

Applying the same technique in McMurdo Sound, Brett et al. (2020, 2024) also used a seawater conductivity of 2,700 mS m^{-1} obtained from extensive oceanographic observations in the region (e.g., Robinson et al., 2014). In Gerlache Inlet, Brogioni et al. (2023) measured seawater salinity of 31.2–32.1 g kg^{-1} in the center and near Tethys Bay on 18 November 2018, corresponding to a slightly lower conductivity of ~2,500 mS m^{-1} (for a temperature of −1.91°C and pressure of 15 dbar) (McDougall & Barker, 2011). However, seawater conductivity in Gerlache Inlet could be variable, and without coincident oceanographic observations, we could only assume a mean seawater conductivity for the entire study region.

5.2. Fast Ice Formation

Fast ice formation during winter in Gerlache Inlet and Silverfish Bay was influenced by coastal morphology and the Terra Nova Bay Polynya. Throughout winter, polynya forcing frequently broke up recently formed fast ice and circulated it eastward where it accumulated along the western boundaries of the Campbell Ice Tongue and Cape Washington. We mostly observed smooth and level fast ice in Gerlache Inlet, indicating predominantly thermodynamic growth. However, rougher dynamically formed fast ice is likely present near Cape Washington and the fast ice edge, as detected with AEM in both bays in 2017 (Langhorne et al., 2023).

The coastline, including the southward protruding ice tongue and Cape Washington, provided anchorage for fast ice as it formed, and once established, protection from katabatic winds and polynya forcing. This was indicated by the fast ice extent in mid-April, which extended to the ice tongue terminus. Reciprocally, the presence of fast ice stabilized the ice tongue as shown by the calving that occurred immediately after the fast ice broke out in January 2021. The coastal fast ice fringe described in Section 4.1 reoccurred over winter in 2021 and was also observed in

late spring of 2005 (Vacchi et al., 2012) and in winter of 2018 (Brogioni et al., 2023), most likely as a result of coastline morphology and shallow bathymetry.

We observed the earliest establishment of fast ice in northeast Gerlache Inlet near the ice tongue where the thickest fast ice and SIPL were measured in late spring (Figures 2b and 2c). Fast ice near the coast likely grows and strengthens more rapidly from heat loss to supercooled ISW and platelet ice consolidation (Gough et al., 2012). Thicker consolidated ice on the *North*, *NS-3*, and *NS-CIT* transects over SIPL maxima near the ice tongue indicated that ISW outflow played an early and significant role in fast ice formation throughout winter. In future studies, ice core texture analysis would constrain the timing and influence of in situ supercooling on consolidated fast ice growth in the region (Dempsey et al., 2010; Langhorne et al., 2015).

5.3. Sub-Ice Platelet Layer Distribution

The distribution of thicker fast ice and SIPL we observed in Gerlache Inlet strongly indicated that in situ supercooled ISW is outflowing from beneath the Campbell Ice Tongue (conjectured as black arrows in Figures 2a and 2c). The SIPL was thickest in the north, northeast, and east near the branch and main flow streams of the ice tongue and decreased in thickness to the west and southwest (Figure 2c). A similar pattern was observed by the AEM surveys in November 2017 (Langhorne et al., 2023). However, our higher resolution in situ study detected multiple narrow (∼100 s m) SIPL maxima south of the branch stream (Figure 6) identifying highly channeled outflow from the ice mélange and grounded regions. Given significant outflow of supercooled ISW, platelet and marine ice potentially contribute to the integrity of the branch stream mélange. Thicker SIPL maxima observed along the main flow stream in transect *NS-CIT* (Figure 5) also suggest that ripple formations in the base of the ice tongue, as observed by Bianchi et al., 2001, could channel ISW outflow. Stevens et al. (2017) conjectured that similar basal channels in the Drygalski Ice Tongue would affect water mass outflow and properties.

Fast ice persistence determines how long platelet ice crystals (once present) can accumulate and grow in situ to form the SIPL. Two months of additional SIPL growth is apparent on all north-south transects (Figures 4 and 5). SIPL thickness decreased significantly from the 6.5 to the 4.5-month fast ice, which strongly indicates that the SIPL was well-established, and of significant thickness in mid-June, prior to the seaward fast ice breaking out. Our EM observations supported the location of grounded regions of the ice tongue from SAR interferometry (Han et al., 2022). The fast ice breakout in mid-June occurred north of where the main flow stream is grounded on a seabed rise (Figures 2 and 5) and the grounded region of the branch stream correlated with thinner SIPL (Figure 6) suggesting hindrance of ISW outflow.

In comparison to the AEM surveys in November 2017 by Langhorne et al. (2023), the SIPL we measured in Gerlache Inlet was thicker and more extensive. However, we could not constrain the overestimate in EM inverted SIPL thickness near the ice tongue or its spatial extent. Additionally, the fast ice was less extensive in November 2017 and had partially broken out from Gerlache Inlet in early September 2017. Considering the previous observations given in Section 2.3, interannual variability in SIPL in this region is expected and could be driven by a combination of factors including wind-forcing on fast ice persistence, variability in snow thickness, and ocean circulation affecting the volumes of in situ supercooled ISW in the region.

5.4. Ice Shelf Water Source Regions and Circulation

Here, we discuss local and regional processes that could contribute to the formation of supercooled ISW and platelet ice in north Terra Nova Bay. The thick fast ice and SIPL we detected in Gerlache Inlet implied that in situ supercooled ISW is abundant to the west of the ice tongue. In Silverfish Bay, the AEM surveys detected a substantially thicker and more extensive SIPL in November 2017 (Langhorne et al., 2023) than Gerlache Inlet signaling that higher volumes of in situ supercooled ISW are outflowing to the east of the ice tongue. These observations show that the ice tongue is a significant source of ISW in north Terra Nova Bay.

The tongue of ISW previously observed near Gerlache Inlet by Budillon and Spezie (2000) had properties that indicated that it was formed by HSSW interaction with glacial ice and pointed to the Campbell Ice Tongue as the source region. Given that the study area is small, and the polynya dominates the fast ice edge in the south, it is plausible that HSSW formed within the polynya could be causing basal melt of the ice tongue at depth and forming ISW.

Bianchi et al. (2001) estimated the grounding line depth of the Campbell Ice Tongue to be ∼700 m and comparable to the Nansen Ice Shelf (660 m) (Frezzotti et al., 2000), which is posited to be the main source of ISW in Terra Nova Bay. The ice tongue thins over a short distance (Bianchi et al., 2001), which provides a steep slope for rapid pressure relief, inducing in situ supercooling, and promoting frazil/platelet ice formation (Jenkins & Bombosch, 1995; Lewis & Perkin, 1986). Basal freezing by ISW (mean rates of 0.75 m a^{-1} and up to 20 m a^{-1}) on the ice tongue has been deduced at ∼400 m depth from SAR interferometry (Han & Lee, 2015). To be in situ supercooled at this depth, ISW would thus have to be of deeper origin than 400 m.

HSSW has been observed in Terra Nova Bay from the seafloor to 400–700 m depth in summer (Yoon et al., 2020) and is more prevalent in winter when sea ice production in the polynya is intense (Ackley et al., 2020). This is deep enough for HSSW to interact with the Campbell Ice Tongue at the 700-m grounding zone. However, other unidentified water masses could also cause basal melting and we emphasize that the region critically needs coincident oceanographic surveying in future studies. We conclude that basal melting of the Campbell Ice Tongue at depth is a significant contributor to ISW in Terra Nova Bay. Our fine scale in situ observations enhance and support the finding of Langhorne et al. (2023) that smaller ice bodies along the Victoria Land Coastline are important contributors to ISW in the western Ross Sea.

5.5. Consequences of Campbell Ice Tongue Degradation

The Campbell Ice Tongue appears to be in a state of change with increased basal melting and decreased ice tongue area. Without anchorage and protection provided by the ice tongue, fast ice establishment and persistence would diminish. Reciprocally, less extensive or thinner fast ice would negatively impact the ice tongue by providing less mechanical reinforcement and increased exposure to winds, ocean swell, and waves as observed by Gomez-Fell et al. (2022) at the Parker Ice Tongue, ∼40 km north of our study region. Collapse of the ice tongue would result in more glacial ice discharge to the ocean and a single wide bay with increased exposure to winds and ocean circulation. Our study shows that reduced ISW formation as a result of ice tongue disintegration would significantly impact the formation and stability of fast ice and SIPL. Lower fast ice persistence would reduce SIPL formation as shown by the thinner SIPL observed beneath the 4.5 versus the 6.5-month fast ice. Platelet ice plays an important role in Antarctic biology by providing a habitat for algae and microorganisms (Arrigo et al., 1993) and nursery for the keystone species Antarctic silverfish (Vacchi et al., 2012). A reduction or disappearance of a SIPL in the study region, the only known nursery for silverfish, would have major implications for the Ross Sea ecosystem. Complex interactions between the ice tongue and fast ice are clearly important not only for the stability of the icescape but for reliant ecosystems.

6. Conclusion

In north Terra Nova Bay, a sub-ice platelet layer (SIPL) occurs beneath fast ice beside the Campbell Ice Tongue, signaling the presence of in situ supercooled ISW in the upper surface ocean. Prior to this study, no dedicated in situ measurement of the thickness distributions of fast ice and SIPL, formed by supercooled ISW circulation, had been carried out and the source of ISW and platelet ice in this region was not well constrained. In late spring of 2021, we carried out drill hole and high-resolution ground-based electromagnetic induction surveys of fast ice and SIPL thickness distributions to infer the pattern of ISW circulation in Gerlache Inlet in north Terra Nova Bay. To characterize the fast ice composition, we monitored fast ice formation throughout the winter of 2021 with satellite observations. We observed that the Terra Nova Bay Polynya has a significant effect on fast ice persistence by breaking it up and circulating it eastward, whereas the western coastline, Campbell Ice Tongue, and Cape Washington provided stabilization. In late spring, thicker fast ice and SIPL were observed near the ice tongue, with very thick and narrow SIPL maxima indicating highly channeled outflow of supercooled ISW, from beneath the ice tongue through ice mélange, subglacial formations, and grounded regions. We conclude that significant volumes of ISW are locally sourced from basal melt of the Campbell Ice Tongue. We identify the need for combined in situ fast ice and oceanographic surveying to fully elucidate the processes at play in this important region. Reciprocal effects observed between the ice tongue, fast ice, and SIPL highlighted the implications of Campbell Ice Tongue degradation for fast ice and SIPL formation and marine species that are highly specialized to this region.

Conflict of Interest

The authors declare no conflicts of interest relevant to this study.

Data Availability Statement

The drill hole (Brett et al., 2025a) and EM (Brett et al., 2025b) data are available at the World Data Center PANGAEA (https://www.pangaea.de). Satellite images were obtained from the European Space Agency (ESA) (through https://search.asf.alaska.edu), the NASA Worldview application (https://worldview.earthdata.nasa.gov/) operated by the NASA/Goddard Space Flight Center Earth Science Data and Information System (EOSDIS) project, and Landsat-8 images courtesy of the U.S. Geological Survey. Multibeam bathymetric data were contributed by Lee et al. (2022) and grounding line data by Han et al. (2022).

Acknowledgments
This research was funded by the New Zealand Antarctic Science Platform's "Opportunities Fund" and logistics support from the Korean Polar Research Institute (KOPRI). It was carried out at Gateway Antarctica, School of Earth and Environment, University of Canterbury, New Zealand. We express our gratitude for the contribution of multibeam bathymetric data from Lee et al. (2022) and grounding line data from Han et al. (2022). We greatly appreciate the invaluable support provided by Ian Hawes and KOPRI Jang Bogo Station staff, in particular, to Land Safety Officer Chiil Ryu, and other field support members.

References

Ackley, S. F., Stammerjohn, S., Maksym, T., Smith, M., Cassano, J., Guest, P., et al. (2020). Sea-ice production and air/ice/ocean/biogeochemistry interactions in the Ross Sea during the PIPERS 2017 autumn field campaign. *Annals of Glaciology*, *61*(82), 181–195. https://doi.org/10.1017/aog.2020.31

Arrigo, K. R., Robinson, D. H., & Sullivan, C. W. (1993). A high resolution study of the platelet ice ecosystem in McMurdo Sound, Antarctica: Photosynthetic and bio-optical characteristics of a dense microalgal bloom. *Marine Ecology Progress Series*, *98*, 173–185. https://doi.org/10.3354/meps098173

Bianchi, C., Chiappini, M., Tabacco, I. E., Passerini, A., Zirizzotti, A., & Zuccheretti, E. (2001). Morphology of bottom surfaces of glacier ice tongues in the East Antarctic region. *Annals of Geophysics*, *1*(44). Retrieved from http://hdl.handle.net/2122/1192

Brett, G. M., Gardiner, N. B., Hawes, I., Kim, S., Rack, W., Irvin, A., et al. (2025a). Drill hole measurements of land-fast sea ice and sub-ice platelet layer thicknesses, fast ice freeboard, and snow depth in Gerlache Inlet, north Terra Nova Bay, Antarctica in November 2021 [Dataset]. *PANGAEA*. https://doi.org/10.1594/PANGAEA.968740

Brett, G. M., Gardiner, N. B., Hawes, I., Kim, S., Rack, W., Irvin, A., et al. (2025b). Late spring 2021 land-fast sea ice and sub-ice platelet layer thicknesses from electromagnetic induction soundings on transects in Gerlache Inlet, Terra Nova Bay, Antarctica [Dataset]. *PANGAEA*. https://doi.org/10.1594/PANGAEA.968714

Brett, G. M., Irvin, A., Rack, W., Haas, C., Langhorne, P. J., & Leonard, G. H. (2020). Variability in the distribution of fast ice and the sub-ice platelet layer near McMurdo Ice Shelf. *Journal of Geophysical Research: Oceans*, *125*(3), e2019JC015678. https://doi.org/10.1029/2019JC015678

Brett, G. M., Leonard, G. H., Rack, W., Haas, C., Langhorne, P. J., Robinson, N., & Irvin, A. (2024). Seasonal and diurnal variability of sub-ice platelet layer thickness in McMurdo Sound from electromagnetic induction sounding. *EGUsphere*, 1–26. https://doi.org/10.5194/egusphere-2023-2724

Brogioni, M., Andrews, M. J., Urbini, S., Jezek, K. C., Johnson, J. T., Leduc-Leballeur, M., et al. (2023). Ice sheet and sea ice Ultrawideband microwave radiometric airborne experiment (ISSIUMAX) in Antarctica: First results from Terra Nova Bay. *The Cryosphere*, *17*(1), 255–278. https://doi.org/10.5194/tc-17-255-2023

Budillon, G., & Spezie, G. (2000). Thermohaline structure and variability in the Terra Nova Bay polynya, Ross Sea. *Antarctic Science*, *12*(4), 493–508. https://doi.org/10.1017/S0954102000000572

Cappelletti, A., Picco, P., & Peluso, T. (2010). Upper ocean layer dynamics and response to atmospheric forcing in the Terra Nova Bay polynya, Antarctica. *Antarctic Science*, *22*(3), 319–329. https://doi.org/10.1017/S095410201000009X

Christie, F. D., Benham, T. J., Batchelor, C. L., Rack, W., Montelli, A., & Dowdeswell, J. A. (2022). Antarctic ice-shelf advance driven by anomalous atmospheric and sea-ice circulation. *Nature Geoscience*, *15*(5), 356–362. https://doi.org/10.1038/s41561-022-00938-x

Dempsey, D. E., Langhorne, P. J., Robinson, N. J., Williams, M. J. M., Haskell, T. G., & Frew, R. D. (2010). Observation and modeling of platelet ice fabric in McMurdo Sound, Antarctica. *Journal of Geophysical Research*, *115*(C1). https://doi.org/10.1029/2008JC005264

Foldvik, A., & Kvinge, T. (1974). Conditional instability of sea water at the freezing point. *Deep-Sea Research and Oceanographic Abstracts*, *21*(3), 169–174. https://doi.org/10.1016/0011-7471(74)90056-4

Fraser, A. D., Ohshima, K. I., Nihashi, S., Massom, R. A., Tamura, T., Nakata, K., et al. (2019). Landfast ice controls on sea-ice production in the Cape Darnley Polynya: A case study. *Remote Sensing of Environment*, *233*, 111315. https://doi.org/10.1016/j.rse.2019.111315

Fraser, A. D., Wongpan, P., Langhorne, P. J., Klekociuk, A. R., Kusahara, K., Lannuzel, D., et al. (2023). Antarctic landfast sea ice: A review of its physics, biogeochemistry and ecology. *Reviews of Geophysics*, *61*(2), e2022RG000770. https://doi.org/10.1029/2022RG000770

Frezzotti, M., Tabacco, I. E., & Zirizzotti, A. (2000). Ice discharge of eastern Dome C drainage area, Antarctica, determined from airborne radar survey and satellite image analysis. *Journal of Glaciology*, *46*(153), 253–264. https://doi.org/10.3189/172756500781832855

Fusco, G., Budillon, G., & Spezie, G. (2009). Surface heat fluxes and thermohaline variability in the Ross Sea and in Terra Nova Bay polynya. *Continental Shelf Research*, *29*(15), 1887–1895. https://doi.org/10.1016/j.csr.2009.07.006

Gerrish, L., Fretwell, P., & Cooper, P. (2022). High resolution vector polylines of the Antarctic coastline (7.6) [Dataset]. *UK Polar Data Centre, Natural Environment Research Council, UK Research & Innovation*. https://doi.org/10.5285/45174e8c-7ce8-4d87-a6f7-570db476c6c9

Giles, A. B., Massom, R. A., & Lytle, V. I. (2008). Fast-ice distribution in East Antarctica during 1997 and 1999 determined using RADARSAT data. *Journal of Geophysical Research*, *113*(C2). https://doi.org/10.1029/2007JC004139

Gomez-Fell, R., Rack, W., Marsh, O. J., & Purdie, H. (2024). Lateral flexure of Erebus Ice Tongue due to ocean current forcing and fast ice coupling. *Journal of Glaciology*, *70*, 1–30. https://doi.org/10.1017/jog.2024.21

Gomez-Fell, R., Rack, W., Purdie, H., & Marsh, O. (2022). Parker Ice Tongue collapse, Antarctica, triggered by loss of stabilizing land-fast sea ice. *Geophysical Research Letters*, *49*(1), e2021GL096156. https://doi.org/10.1029/2021GL096156

Gough, A. J., Mahoney, A. R., Langhorne, P. J., Williams, M. J., Robinson, N. J., & Haskell, T. G. (2012). Signatures of supercooling: McMurdo Sound platelet ice. *Journal of Glaciology*, *58*(207), 38–50. https://doi.org/10.3189/2012JoG10J218

Greene, C. A., Young, D. A., Gwyther, D. E., Galton-Fenzi, B. K., & Blankenship, D. D. (2018). Seasonal dynamics of Totten Ice Shelf controlled by sea ice buttressing. *The Cryosphere*, *12*(9), 2869–2882. https://doi.org/10.5194/tc-12-2869-2018

Guglielmo, L., Zagami, G., Saggiomo, V., Catalano, G., & Granata, A. (2007). Copepods in spring annual sea ice at Terra Nova Bay (Ross Sea, Antarctica). *Polar Biology*, *30*(6), 747–758. https://doi.org/10.1007/s00300-006-0234-2

Haas, C., Langhorne, P. J., Rack, W., Leonard, G. H., Brett, G. M., Price, D., et al. (2021). Airborne mapping of the sub-ice platelet layer under fast ice in McMurdo Sound, Antarctica. *The Cryosphere*, *15*(1), 247–264. https://doi.org/10.5194/tc-15-247-2021

Han, H., Kim, S. H., & Kim, S. (2022). Decadal changes of Campbell Glacier Tongue in East Antarctica from 2010 to 2020 and implications of ice pinning conditions analyzed by optical and SAR datasets. *GIScience & Remote Sensing*, *59*(1), 705–721. https://doi.org/10.1080/15481603.2022.2055380

Han, H., & Lee, H. (2014). Tide deflection of Campbell Glacier Tongue, Antarctica, analyzed by double-differential SAR interferometry and finite element method. *Remote Sensing of Environment*, *141*, 201–213. https://doi.org/10.1016/j.rse.2013.11.002

Han, H., & Lee, H. (2015). Tide-corrected flow velocity and mass balance of Campbell Glacier Tongue, East Antarctica, derived from interferometric SAR. *Remote Sensing of Environment*, *160*, 180–192. https://doi.org/10.1016/j.rse.2015.01.014

Han, H., & Lee, H. (2018). Glacial and tidal strain of landfast sea ice in Terra Nova Bay, East Antarctica, observed by interferometric SAR techniques. *Remote Sensing of Environment*, *209*, 41–51. https://doi.org/10.1016/j.rse.2018.02.033

Hellmer, H. H. (2004). Impact of Antarctic ice shelf basal melting on sea ice and deep ocean properties. *Geophysical Research Letters*, *31*(10). https://doi.org/10.1029/2004GL019506

Holland, P. R., & Feltham, D. L. (2005). Frazil dynamics and precipitation in a water column with depth-dependent supercooling. *Journal of Fluid Mechanics*, *530*, 101–124. https://doi.org/10.1017/S002211200400285X

Hoppmann, M., Nicolaus, M., Hunkeler, P. A., Heil, P., Behrens, L. K., König-Langlo, G., & Gerdes, R. (2015). Seasonal evolution of an ice-shelf influenced fast-ice regime, derived from an autonomous thermistor chain. *Journal of Geophysical Research: Oceans*, *120*(3), 1703–1724. https://doi.org/10.1002/2014JC010327

Hoppmann, M., Nicolaus, M., Paul, S., Hunkeler, P. A., Heinemann, G., Willmes, S., et al. (2015). Ice platelets below Weddell Sea landfast sea ice. *Annals of Glaciology*, *56*(69), 175–190. https://doi.org/10.3189/2015AoG69A678

Hughes, K., Langhorne, P., Leonard, G., & Stevens, C. (2014). Extension of an Ice Shelf Water plume model beneath sea ice with application in McMurdo Sound, Antarctica. *Journal of Geophysical Research: Oceans*, *119*(12), 8662–8687. https://doi.org/10.1002/2013JC009411

Irvin, A. (2018). *Towards multi-channel inversion of electromagnetic sea ice surveys* (Published doctoral thesis). York University. Toronto, Canada. Retrieved from http://hdl.handle.net/10315/35925

Jacobs, S. S., Fairbanks, R. G., & Horibe, Y. (1985). Origin and evolution of water masses near the Antarctic continental margin: Evidence from $H_2{}^{18}O/H_2{}^{16}O$ ratios in seawater. *Oceanology of the Antarctic Continental Shelf*, *43*, 59–85. https://doi.org/10.1029/AR043p0059

Jenkins, A., & Bombosch, A. (1995). Modeling the effects of frazil ice crystals on the dynamics and thermodynamics of ice shelf water plumes. *Journal of Geophysical Research*, *100*(C4), 6967–6981. https://doi.org/10.1029/94JC03227

Jung, J., Ko, Y., Lee, J., Yang, K., Park, Y. K., Kim, S., et al. (2021). Multibeam bathymetry and distribution of clay minerals on surface sediments of a small bay in Terra Nova Bay, Antarctica. *Minerals*, *11*(1), 72. https://doi.org/10.3390/min11010072

Kurtz, D. D., & Bromwich, D. H. (1985). A recurring, atmospherically forced polynya in Terra Nova Bay. *Oceanology of the Antarctic Continental Shelf*, *43*, 177–201. https://doi.org/10.1029/AR043p0177

Langhorne, P. J., Haas, C., Price, D., Rack, W., Leonard, G. H., Brett, G. M., & Urbini, S. (2023). Fast ice thickness distribution in the western Ross Sea in late spring. *Journal of Geophysical Research: Oceans*, *128*(2), e2022JC019459. https://doi.org/10.1029/2022JC019459

Langhorne, P. J., Hughes, K. G., Gough, A. J., Smith, I. J., Williams, M. J. M., Robinson, N. J., et al. (2015). Observed platelet ice distributions in Antarctic sea ice: An index for ocean-ice shelf heat flux. *Geophysical Research Letters*, *42*(13), 5442–5451. https://doi.org/10.1002/2015GL064508

Lazzara, L., Nardello, I., Ermanni, C., Mangoni, O., & Saggiomo, V. (2007). Light environment and seasonal dynamics of microalgae in the annual sea ice at Terra Nova Bay, Ross Sea, Antarctica. *Antarctic Science*, *19*(1), 83–92. https://doi.org/10.1017/S0954102007000119

Lee, J., Kim, S., Moon, H., Kim, H. J., & Yoo, K. C. (2022). Multibeam bathymetry and distribution of clay minerals on surface sediments of a small bay in Terra Nova Bay, Antarctica [Dataset]. *Korean Polar Research Institute Abstract Collection*. 31.

Lewis, E., & Perkin, R. (1985). The winter oceanography of McMurdo Sound, Antarctica. *Oceanology of the Antarctic Continental Shelf*, 145–165. https://doi.org/10.1029/AR043p0145

Lewis, E., & Perkin, R. (1986). Ice pumps and their rates. *Journal of Geophysical Research*, *91*(C10), 11756–11762. https://doi.org/10.1029/JC091iC10p11756

Massom, R. A., Giles, A. B., Fricker, H. A., Warner, R. C., Legrésy, B., Hyland, G., et al. (2010). Examining the interaction between multi-year landfast sea ice and the Mertz Glacier Tongue, East Antarctica: Another factor in ice sheet stability? *Journal of Geophysical Research*, *115*(C12). https://doi.org/10.1029/2009JC006083

Massom, R. A., Scambos, T. A., Bennetts, L. G., Reid, P., Squire, V. A., & Stammerjohn, S. E. (2018). Antarctic ice shelf disintegration triggered by sea ice loss and ocean swell. *Nature*, *558*(7710), 383–389. https://doi.org/10.1038/s41586-018-0212-1

McDougall, T. J., & Barker, P. M. (2011). Getting started with TEOS-10 and the Gibbs Seawater (GSW) oceanographic toolbox. *Scor/Iapso WG*, *127*(532), 1–28.

Nakata, K., Ohshima, K. I., Nihashi, S., Kimura, N., & Tamura, T. (2015). Variability and ice production budget in the Ross Ice Shelf Polynya based on a simplified polynya model and satellite observations. *Journal of Geophysical Research: Oceans*, *120*(9), 6234–6252. https://doi.org/10.1002/2015JC010894

Nihashi, S., & Ohshima, K. I. (2015). Circumpolar mapping of Antarctic coastal polynyas and landfast sea ice: Relationship and variability. *Journal of Climate*, *28*(9), 3650–3670. https://doi.org/10.1175/JCLI-D-14-00369.1

Price, D., Rack, W., Langhorne, P. J., Haas, C., Leonard, G., & Barnsdale, K. (2014). The sub-ice platelet layer and its influence on freeboard to thickness conversion of Antarctic sea ice. *The Cryosphere*, *8*(3), 1031–1039. https://doi.org/10.5194/tc-8-1031-2014

Purdie, C. R., Langhorne, P. J., Leonard, G. H., & Haskell, T. G. (2006). Growth of first-year landfast Antarctic sea ice determined from winter temperature measurements. *Annals of Glaciology*, *44*, 170–176. https://doi.org/10.3189/172756406781811853

Robinson, N. J., Williams, M. J., Stevens, C. L., Langhorne, P. J., & Haskell, T. G. (2014). Evolution of a supercooled Ice Shelf Water plume with an actively growing sub-ice platelet matrix. *Journal of Geophysical Research: Oceans*, *119*(6), 3425–3446. https://doi.org/10.1002/2013JC009399

Rusciano, E., Budillon, G., Fusco, G., & Spezie, G. (2013). Evidence of atmosphere–sea ice–ocean coupling in the Terra Nova Bay polynya (Ross Sea—Antarctica). *Continental Shelf Research*, *61*, 112–124. https://doi.org/10.1016/j.csr.2013.04.002

Smith, I. J., Langhorne, P. J., Frew, R. D., Vennell, R., & Haskell, T. G. (2012). Sea ice growth rates near ice shelves. *Cold Regions Science and Technology*, *83*, 57–70. https://doi.org/10.1016/j.coldregions.2012.06.005

Souchez, R., Tison, J. L., Lorrain, R., Fléhoc, C., Stiévenard, M., Jouzel, J., & Maggi, V. (1995). Investigating processes of marine ice formation in a floating ice tongue by a high-resolution isotopic study. *Journal of Geophysical Research*, *100*(C4), 7019–7025. https://doi.org/10.1029/95JC00142

Stevens, C., Lee, W. S., Fusco, G., Yun, S., Grant, B., Robinson, N., & Hwang, C. Y. (2017). The influence of the Drygalski Ice Tongue on the local ocean. *Annals of Glaciology*, *58*(74), 51–59. https://doi.org/10.1017/aog.2017.4

Thompson, L., Smith, M., Thomson, J., Stammerjohn, S., Ackley, S., & Loose, B. (2020). Frazil ice growth and production during katabatic wind events in the Ross Sea, Antarctica. *The Cryosphere*, *14*(10), 3329–3347. https://doi.org/10.5194/tc-14-3329-2020

Vacchi, M., DeVries, A. L., Evans, C. W., Bottaro, M., Ghigliotti, L., Cutroneo, L., & Pisano, E. (2012). A nursery area for the Antarctic silverfish *Pleuragramma antarcticum* at Terra Nova Bay (Ross Sea): First estimate of distribution and abundance of eggs and larvae under the seasonal sea-ice. *Polar Biology*, *35*(10), 1573–1585. https://doi.org/10.1007/s00300-012-1199-y

Vacchi, M., La Mesa, M., Dalu, M., & MacDonald, J. (2004). Early life stages in the life cycle of Antarctic silverfish, *Pleuragramma antarcticum* in Terra Nova Bay, Ross Sea. *Antarctic Science*, *16*(3), 299–305. https://doi.org/10.1017/S0954102004002135

Wongpan, P., Langhorne, P. J., Dempsey, D. E., Hahn-Woernle, L., & Sun, Z. (2015). Simulation of the crystal growth of platelet sea ice with diffusive heat and mass transfer. *Annals of Glaciology*, *56*(69), 127–136. https://doi.org/10.3189/2015AoG69A777

Wongpan, P., Vancoppenolle, M., Langhorne, P. J., Smith, I. J., Madec, G., Gough, A. J., et al. (2021). Sub-ice platelet layer physics: Insights from a mushy-layer sea ice model. *Journal of Geophysical Research: Oceans*, *126*(6), e2019JC015918. https://doi.org/10.1029/2019JC015918

Yoon, S. T., Lee, W. S., Stevens, C., Jendersie, S., Nam, S., Yun, S., et al. (2020). Variability in high-salinity shelf water production in the Terra Nova Bay polynya, Antarctica. *Ocean Science*, *16*(2), 373–388. https://doi.org/10.5194/os-16-373-2020